

Enhanced ionic conductivity of protonated antiperovskite via tuning lattice and rotational dynamics

*Chaohong Guan, Yu Yang, Runxin Ouyang, Huirong Jing, Jieqiong Yan, Hong Zhu**

University of Michigan–Shanghai Jiao Tong University Joint Institute, Shanghai Jiao Tong
University, Shanghai 200240, China

S1. Predicting the ground state structure of studied electrolytes

S1.1 Li₂OHCl

Based on the mentioned in the introduction, the low-temperature phase of Li₂OHCl is the orthorhombic phase (Amm2 and Pban space groups), the phase transition will occur with the increased temperature (> 30 °C), forming the cubic phase at higher temperature. Hence, in this work, the orthorhombic and cubic phases were considered for the searching of ground state structure.

According to the method shown in reference, firstly, based on the Wyckoff positions of all atoms of Li₂OHCl reported by Hanghofer et al.[1], we built a 2*2*2 supercell (model 1, Pban space group) with the experimental lattice constants. Then, considering the partial occupancy of Li and H atoms, 20000 structures from the parent partially occupied supercell were randomly sampled and their electrostatic energy was calculated, as implemented in the pymatgen code[2]. Then, 20 structures with the lowest electrostatic energy were relaxed by DFT.

Additionally, the similar method was adopted to build the 3*3*3 cubic Li₂OHCl (model 2). We firstly built the Li₃OCl unit cell by the experiment lattice constants, and the 2/3 partial occupancy was considered to the 3d Li sites in Li₃OCl. Specially, the H atom were randomly placed 0.98 Å away from each oxygen atom, and 20000 random structures also were built, the electrostatic energy of these structures were calculated and the 20 structures with the lowest electrostatic energy were relaxed by DFT.

The obtained ground state energy for both models are -4.55 and -4.58 eV/atom, respectively, hence, the final ground state structure was based on model 2, and after relaxation, the structure became tetragonal with slight distortion, as shown in Table S1, the result is consistent well with the work of Dawson et al. [3]

Table S1 Lattice parameters of the ground state structure of Li₂OHCl.

	a/Å	b/Å	c/Å	α/°	β/°	γ/°
This work	3.86	3.57	3.86	90	90	90
Reference 3	3.853	3.591	3.853	90	90	90

S1.2 Brominated Li₂OHCl

In this work, the ground state structures of brominated Li_2OHCl were built as follows. Firstly, based on the ground state structure of model 2, the same initial structure was selected to determine the ground state structure of brominated Li_2OHCl . For $\text{Li}_2\text{OHBr}_{0.1}\text{Cl}_{0.9}$, 3 of the 27 chlorine atoms in the supercell were replaced by Br in the $3 \times 3 \times 3$ supercell (containing 135 atoms), which means the $\text{Li}_{54}(\text{OH})_{27}\text{Br}_3\text{Cl}_{24}$ composition for $\text{Li}_2\text{OHBr}_{0.1}\text{Cl}_{0.9}$ was simulated. Notably, this substitution will generate 2925 structures with the same electrostatic energies and therefore, the MatErials Graph Network (MEGNet) model [4] was adopted to predict the formation energies of these structures. Then, the 20 structures with the lowest formation energy were relaxed by DFT to obtain the final structure. A similar procedure was adopted to determine the ground state structure of $\text{Li}_2(\text{OH})_{0.9}\text{Br}_{0.1}\text{Cl}$, 3 of 27 OH groups were replaced by Br, which means the $\text{Li}_{54}(\text{OH})_{24}\text{Br}_3\text{Cl}_{27}$ composition was simulated. The obtained ground state structures of $\text{Li}_2\text{OHBr}_{0.1}\text{Cl}_{0.9}$ and $\text{Li}_2(\text{OH})_{0.9}\text{Br}_{0.1}\text{Cl}$ are shown in Figure S1a and b, the both structures are pseudo-cubic, and their lattice parameters are listed in Table S2,

Table S2 Lattice parameters of the ground state structure of $\text{Li}_2\text{OHBr}_{0.1}\text{Cl}_{0.9}$ and $\text{Li}_2(\text{OH})_{0.9}\text{Br}_{0.1}\text{Cl}$.

System	a/Å	b/Å	c/Å	α	β	γ
$\text{Li}_2\text{OHBr}_{0.1}\text{Cl}_{0.9}$	3.86	3.92	3.86	90.00	89.99	89.99
$\text{Li}_2(\text{OH})_{0.9}\text{Br}_{0.1}\text{Cl}$	3.91	3.93	3.91	89.99	90.00	90.01

S2. Computational methods

2.1 Phase Stability

The compositional stability of Li₂OHCl-based electrolytes was assessed by comparing the normalized ground-state energy to that of all phases in the Li-H-O-Cl-Br compositional space[5] which can be defined as $E = E_{GS}/N_{atom}$, the N_{atom} represents the number of atoms in the crystal. In addition, the phase diagrams were constructed by computing the convex hull for all structures. The stable compositions are located on the hull, the energy of above hull of metastable structure lie above the hull, $E_{hull} > 0$.

2.2 Electrochemical Stability

Two approaches were adopted to assess the electrochemical stabilities of the Li₂OHCl-based APs. Firstly, the band gap of each APs was calculated based on the HSE06 hybrid functional.[6] Notably, according to the previous studies, this method provides an upper limit to the electrochemical window.[7, 8] Another approach to assess the stability is based on the grand potential phase diagram (GPPD)[9]. The electrolyte is taken to be an open system to Li and the equilibrium phases formed at the electrode/electrolyte interface for different Li chemical potentials can be computed, and the electrochemical window is the range of Li chemical potential from the critical reduced Li potential to the critical oxidized potential.

2.3 Elastic moduli estimation from the elastic tensor

To estimate the elastic moduli (including bulk, B, shear, G, and Young, E, moduli) of our studied APs, the Voigt-Reuss-Hill approximation[10] was adopted to computed the elastic tensor, C_{ij} , the corresponding calculated process are shown in the following:

$$B_V = \frac{(C_{11} + C_{22} + C_{33}) + 2(C_{12} + C_{23} + C_{31})}{9}$$
$$G_V = \frac{(C_{11} + C_{22} + C_{33}) - (C_{12} + C_{23} + C_{31}) + 3(C_{44} + C_{55} + C_{66})}{15}$$

Then, according the Reuss approximation, the B_R and G_R were calculated by the compliance tensor,

$$S_{ij} = C_{ij}^{-1}, \text{ as}$$

$$B_R = \frac{1}{(S_{11} + S_{22} + S_{33}) + 2(S_{12} + S_{23} + S_{31})}$$

$$G_R = \frac{1}{4(S_{11} + S_{22} + S_{33}) - 4(S_{12} + S_{23} + S_{31}) + 3(S_{44} + S_{55} + S_{66})}$$

Therefore, the elastic moduli B and G were obtained:

$$B = \frac{(B_V + B_R)}{2}$$

$$G = \frac{(G_V + G_R)}{2}$$

And the E was estimated as

$$E = \frac{9BG}{(3B + G)}$$

Table S3 Mechanical properties of APs studied in our work.

	Li ₃ OCl	Li ₂ OHCl	Li ₂ OHBr _{0.1} Cl _{0.9}	Li ₂ (OH) _{0.9} Br _{0.1} Cl
B	48.21	34.61	40.25	42.6
E	86.53	54.44	55.15	53.93
G	36.03	21.99	21.69	20.92
G/B	0.75	0.64	0.53	0.49

Table S4 The detailed data of total elastic moduli for studied structures (Gpa).

	C11	C22	C33	C12	C23	C31	C44	C55	C66
Li ₂ OHCl	107.2	65.1	106	39	37.7	68.8	34.5	35	54.7
Li ₂ OHBr _{0.1} Cl _{0.9}	105	62.4	104.2	56.8	53.4	82.2	43.4	44.8	63.7
Li ₂ (OH) _{0.9} Br _{0.1} Cl	106.7	63.5	104.2	61.4	59.3	87.7	44.7	44.2	62.2

2.4 Bader charge analysis

In this work, the bader charge analysis was calculated to study the charge distribution and ionicity of these Li₂OHCl-based solid state electrolytes. The average Bader charges of different atoms for Li₂OHCl, Li₂OHBr_{0.1}Cl_{0.9} and Li₂(OH)_{0.9}Br_{0.1}Cl are shown in Table S5.

Table S5 Bader charges of Li₂OHCl, Li₂OHBr_{0.1}Cl_{0.9} and Li₂(OH)_{0.9}Br_{0.1}Cl.

	Li ₂ OHCl	Li ₂ OHBr _{0.1} Cl _{0.9}	Li ₂ (OH) _{0.9} Br _{0.1} Cl
Li	0.86	0.86	0.86

H	0.54	0.55	0.56
Cl	-0.85	-0.84	-0.84
O	-1.41	-1.43	-1.45
Br		-0.81	-0.80

2.5 Ab initio molecular dynamics simulation (AIMD)

Ab initio molecular dynamics (AIMD), initialized from the lowest-energy atomic configurations, was used to investigate the ionic conductivity. All AIMD simulations (Li vacancies are created) are performed in an NVT ensemble with a timestep of 2 fs and using a Nosé–Hoover thermostat[11] for a period of 80ps. A minimal Γ -point-only k-point grid was used with spin-polarized calculations. The AIMD simulations were run at 800, 900, 1000, 1100 and 1200 K. All the data were fitted assuming Arrhenius behavior to obtain the activation energy and ionic conductivity at 373 K. To gain insight into the diffusion mechanism, the AIMD trajectories were analyzed to identify the Li jumps and the time scale of the OH reorientations. Details about the method are given in the following. The mean-square displacement (MSD) of the Li ions was estimated from[12]

$$MSD_{Li}(t) = \frac{1}{N} \sum_{i=1}^N |r_i(t + t_0) - r_i(t_0)|^2$$

According to the MSD, the self-diffusion coefficient was estimated using

$$D_{Li} = \frac{MSD_{Li}}{6t} = D_{Li}^0 \exp\left(-\frac{E_a}{k_B T}\right)$$

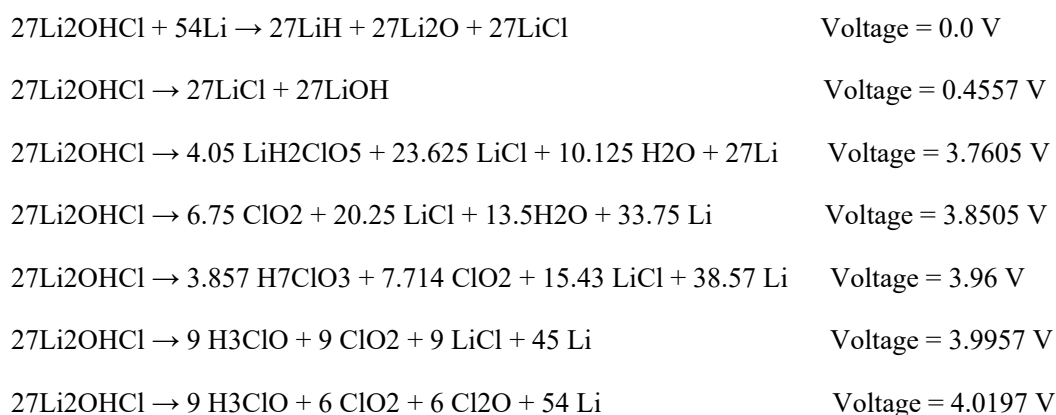
Where D_{Li}^0 is a pre-factor, k_B is the Boltzmann's constant, T is the simulation temperature in K, and E_a is the activation energy. Following, the temperature-dependent ionic conductivity, $\sigma_{Li}(T)$, was estimated from the Nernst-Einstein relation[13] as

$$\sigma_{Li}(T) = \frac{(Z_{Li}e)^2 N D_{Li}}{V k_B T}$$

Where Z_{Li} is the integer charge of a Li ion and V is the volume of the simulation box. The MSD and the pair radial distribution function was calculated by pymatgenn diffusion package[2].

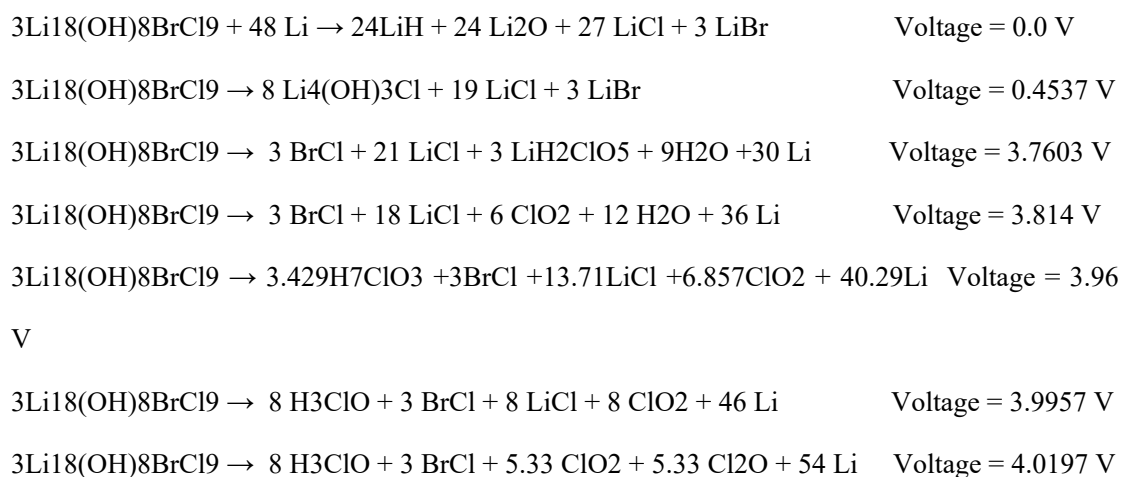
S3. The decomposition reactions of SSEs with lithium metal

S3.1 Decomposition reactions of Li₂OHCl with lithium metal



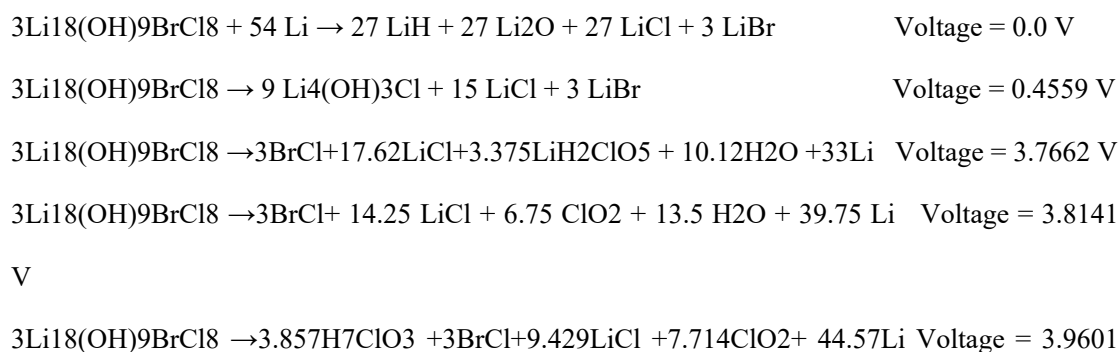
S3.2 Decomposition reactions of Li₂(OH)_{0.9}Br_{0.1}Cl with lithium metal

Because the bulk of Li₂(OH)_{0.9}Br_{0.1}Cl is 3 × 3 × 3 supercell, hence:



S3.3 Decomposition reactions of Li₂(OH)_{0.9}Br_{0.1}Cl with lithium metal

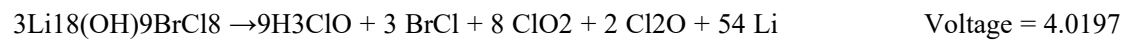
Because the bulk of Li₂OHBr_{0.1}Cl_{0.9} is 3 × 3 × 3 supercell, hence:



V



V



V

S4. Analysis of the trajectories from the AIMD simulations

Firstly, the lithium atoms in the studied APs can be labeled as shown in Figure S10a, it is noted that the label is the nearest-neighbor site. Considering the situation for the exist of 1/3 Li vacancies in the Li_2OHCl -based electrolytes, we drew a lattice of 9 available Li sites and 6 Li ions. The 6 Li ions occupy 6 sites of the total 9 sites. During the label process, the distance (d) between Li ion and Li sites was estimated. The site, d s that has an ion closest to it will be given the label specific to that ion. denotes the label of the L_s^j Li ion assigned to the site at the time instant j . The length of the L_s^j vector (for j fixed) is 81 for the studied electrolytes as the defect-free Li_3OCl lattice has 81 available Li sites in the $3 \times 3 \times 3$ supercell. Thus, $L_s^j \in [14...54]$ since 54 ions are present and $L_{s=0}^j$ are the unoccupied sites. The method also was adopted by the previous studied.

Then, to count the Li hops, the $m = |L_s^{j+1} - L_s^j|$ has been calculated, as shown in Figure S6b and c, if the m does not equal to 0, the Li jump occurred. And when $m = 2$ indicates that a single Li ion hops between two vacant sites. Detailly, we note that the solid-line arrow in the left-hand part of Figure S5b shows an event where one Li ion (No.2) jumps from an occupied site (No.5) to a vacant site (No. 8). We note that two labels (L5 and L8) changed. Similarly, if two Li ions jump from two occupied sites to two vacant sites, there will be a change of 4 labels. Therefore, an even number of labels change ($m=4$) can represent a mode of jumps where Li ions move from occupied sites to vacant sites. The number of atoms jumping during such an event is $n = m/2$, can be called: individual hopping.

Besides the individual hop, the concurrent hop will also be considered in this work, seeing the dashed arrow in the Figure S6b, when Li ion No.2 occupies the vacant site No.8, site 5 is vacant and No.5 Li ion jumps to occupy it, leaving its site (No.2). The occurrence of the event represented by the dashed-line arrow depends on the occurrence of the event represented by the solid-line arrow. In addition, we quantified the number of jumps occurring at each Li site within

the lattice. In this case, the $\sum_{j=0}^T (|L_s^{j+1} - L_s^j| \neq 0)$ was calculated for each s , where T is the total number of steps analyzed.

In addition, the orientational correlation function was calculated to analyze the timescales of

OH groups reorientation of the studied APs [15]:

$$C_n(t) = \langle \rho [P_n(u(0) \cdot u(t))] \rangle$$

Where ρ is the autocorrelation, P_n is the n^{th} order Legendre's polynomial, $u(0) \cdot u(t)$ is the argument of the polynomial where $u(t)$ is the unit vector at time t .

S5. The coordinates of our studied structures

Li2OHCl				Li ₂ (OH) _{0.9} Br _{0.1} Cl				Li ₂ OHBBr _{0.1} Cl _{0.9}			
a/Å		b/Å		c/Å		a/Å		b/Å		c/Å	
3.86		3.57		3.86		11.73		11.79		11.73	
α		β		γ		α		β		γ	
90°		90°		90°		89.99		90.00		90.01	
	x	y	z		x	y	z		x	y	z
Li1	1.0	0.443	0.500	Li1	0.329	0.152	0.170	Li1	0.333	0.141	0.166
Li2	0.5	0.440	0	Li2	0.329	0.152	0.494	Li2	0.333	0.149	0.497
Cl1	1.0	0.530	0.5	Li3	0.310	0.118	0.835	Li3	0.333	0.150	0.837
O1	0.5	0.53	0.5	Li4	0.353	0.462	0.170	Li4	0.333	0.474	0.166
H1	0.5	0.804	0.5	Li5	0.335	0.488	0.503	Li5	0.333	0.476	0.501
				Li6	0.337	0.467	0.829	Li6	0.334	0.475	0.833
				Li7	0.333	0.791	0.165	Li7	0.334	0.809	0.167
				Li8	0.336	0.813	0.502	Li8	0.333	0.808	0.500
				Li9	0.335	0.811	0.835	Li9	0.334	0.807	0.833
				Li10	0.669	0.154	0.169	Li10	0.667	0.141	0.167
				Li11	0.670	0.134	0.496	Li11	0.667	0.141	0.500
				Li12	0.687	0.129	0.837	Li12	0.667	0.142	0.834
				Li13	0.669	0.480	0.169	Li13	0.666	0.482	0.163
				Li14	0.668	0.478	0.502	Li14	0.667	0.483	0.504
				Li15	0.666	0.458	0.831	Li15	0.666	0.475	0.833
				Li16	0.663	0.819	0.161	Li16	0.667	0.809	0.168
				Li17	0.643	0.784	0.502	Li17	0.667	0.809	0.500
				Li18	0.662	0.819	0.837	Li18	0.667	0.807	0.833
				Li19	0.002	0.145	0.169	Li19	0.000	0.142	0.166
				Li20	1.000	0.124	0.498	Li20	0.000	0.141	0.500
				Li21	0.003	0.147	0.835	Li21	0.000	0.143	0.834
				Li22	0.977	0.451	0.168	Li22	0.000	0.474	0.166
				Li23	0.996	0.485	0.503	Li23	0.000	0.476	0.501
				Li24	0.996	0.486	0.827	Li24	0.000	0.475	0.833
				Li25	0.004	0.801	0.163	Li25	1.000	0.817	0.170
				Li26	0.020	0.796	0.503	Li26	1.000	0.808	0.500
				Li27	0.002	0.821	0.836	Li27	1.000	0.815	0.830
				Li28	0.163	0.152	0.005	Li28	0.166	0.143	0.000
				Li29	0.165	0.145	0.332	Li29	0.166	0.142	0.333
				Li30	0.164	0.154	0.665	Li30	0.163	0.150	0.667
				Li31	0.163	0.462	0.980	Li31	0.167	0.475	0.000
				Li32	0.165	0.451	0.357	Li32	0.167	0.475	0.334
				Li33	0.165	0.480	0.664	Li33	0.167	0.475	0.667
				Li34	0.169	0.791	0.000	Li34	0.170	0.815	0.000
				Li35	0.171	0.801	0.330	Li35	0.167	0.807	0.333
				Li36	0.173	0.819	0.671	Li36	0.167	0.807	0.666
				Li37	0.498	0.118	0.023	Li37	0.500	0.141	0.000
				Li38	0.498	0.147	0.331	Li38	0.500	0.141	0.333
				Li39	0.497	0.129	0.647	Li39	0.503	0.149	0.667
				Li40	0.504	0.467	0.996	Li40	0.499	0.476	0.000
				Li41	0.506	0.486	0.337	Li41	0.497	0.483	0.334
				Li42	0.502	0.458	0.667	Li42	0.499	0.476	0.667
				Li43	0.498	0.811	0.998	Li43	0.500	0.808	0.000
				Li44	0.497	0.821	0.331	Li44	0.500	0.809	0.333
				Li45	0.497	0.819	0.671	Li45	0.500	0.808	0.667
				Li46	0.839	0.152	0.004	Li46	0.834	0.142	0.000
				Li47	0.836	0.124	0.334	Li47	0.834	0.141	0.333
				Li48	0.837	0.134	0.663	Li48	0.834	0.141	0.667
				Li49	0.831	0.488	0.998	Li49	0.834	0.474	0.000
				Li50	0.830	0.485	0.338	Li50	0.837	0.482	0.334
				Li51	0.831	0.478	0.665	Li51	0.834	0.474	0.667
				Li52	0.831	0.813	0.997	Li52	0.830	0.817	0.000

				Li53	0.830	0.796	0.313	Li53	0.833	0.809	0.333
				Li54	0.832	0.784	0.690	Li54	0.833	0.809	0.666
				H1	0.167	0.272	0.166	H1	0.167	0.262	0.167
				H2	0.154	0.261	0.499	H2	0.164	0.264	0.497
				H3	0.176	0.265	0.834	H3	0.164	0.265	0.836
				H4	0.166	0.598	0.491	H4	0.167	0.593	0.167
				H5	0.174	0.593	0.830	H5	0.166	0.596	0.500
				H6	0.172	0.917	0.161	H6	0.167	0.593	0.833
				H7	0.170	0.926	0.493	H7	0.170	0.931	0.170
				H8	0.167	0.928	0.846	H8	0.167	0.926	0.500
				H9	0.500	0.265	0.157	H9	0.169	0.928	0.831
				H10	0.507	0.259	0.497	H10	0.500	0.259	0.166
				H11	0.503	0.593	0.159	H11	0.502	0.262	0.498
				H12	0.501	0.594	0.513	H12	0.503	0.264	0.836
				H13	0.505	0.583	0.828	H13	0.497	0.597	0.164
				H14	0.487	0.928	0.166	H14	0.497	0.598	0.503
				H15	0.509	0.932	0.500	H15	0.500	0.596	0.834
				H16	0.500	0.939	0.833	H16	0.500	0.929	0.167
				H17	0.834	0.261	0.179	H17	0.500	0.926	0.500
				H18	0.839	0.250	0.495	H18	0.500	0.926	0.833
				H19	0.836	0.259	0.826	H19	0.833	0.260	0.167
				H20	0.843	0.598	0.167	H20	0.834	0.259	0.500
				H21	0.834	0.606	0.500	H21	0.833	0.262	0.834
				H22	0.821	0.594	0.833	H22	0.836	0.595	0.164
				H23	0.841	0.926	0.164	H23	0.836	0.597	0.503
				H24	0.833	0.932	0.824	H24	0.833	0.593	0.833
				Br1	0.162	0.543	0.171	H25	0.831	0.931	0.169
				Br2	0.496	0.210	0.838	H26	0.833	0.929	0.500
				Br3	0.829	0.876	0.504	H27	0.830	0.931	0.830
				Cl1	0.324	0.017	0.009	Br1	0.333	0.008	0.667
				Cl2	0.331	0.022	0.332	Br2	0.666	0.342	0.334
				Cl3	0.327	0.018	0.661	Br3	1.000	0.675	0.000
				Cl4	0.326	0.353	0.007	Cl1	0.332	0.017	0.001
				Cl5	0.339	0.351	0.340	Cl2	0.333	0.017	0.334
				Cl6	0.322	0.353	0.655	Cl3	0.334	0.349	0.000
				Cl7	0.344	0.682	0.989	Cl4	0.334	0.350	0.334
				Cl8	0.345	0.687	0.344	Cl5	0.334	0.349	0.666
				Cl9	0.335	0.689	0.669	Cl6	0.333	0.684	0.001
				Cl10	0.672	0.018	0.007	Cl7	0.334	0.683	0.333
				Cl11	0.656	0.020	0.322	Cl8	0.333	0.681	0.667
				Cl12	0.659	0.020	0.674	Cl9	0.667	0.016	0.000
				Cl13	0.678	0.353	0.011	Cl10	0.667	0.014	0.333
				Cl14	0.669	0.356	0.336	Cl11	0.666	0.017	0.667
				Cl15	0.678	0.349	0.656	Cl12	0.666	0.351	0.000
				Cl16	0.664	0.689	0.998	Cl13	0.666	0.350	0.666
				Cl17	0.660	0.685	0.328	Cl14	0.667	0.684	0.001
				Cl18	0.657	0.683	0.676	Cl15	0.667	0.682	0.333
				Cl19	0.002	0.022	0.002	Cl16	0.667	0.683	0.666
				Cl20	0.011	0.015	0.322	Cl17	0.000	0.015	0.000
				Cl21	0.012	0.020	0.678	Cl18	0.000	0.016	0.333
				Cl22	0.993	0.351	0.994	Cl19	0.001	0.017	0.668
				Cl23	0.991	0.350	0.343	Cl20	0.000	0.348	0.000
				Cl24	0.998	0.356	0.665	Cl21	0.000	0.351	0.334
				Cl25	0.989	0.687	0.988	Cl22	0.000	0.349	0.666
				Cl26	0.993	0.687	0.341	Cl23	0.999	0.684	0.333
				Cl27	0.006	0.685	0.673	Cl24	0.001	0.684	0.667
				O1	0.165	0.190	0.169	H1	0.166	0.180	0.167
				O2	0.162	0.179	0.497	H2	0.165	0.182	0.499
				O3	0.165	0.183	0.836	H3	0.166	0.182	0.834
				O4	0.164	0.517	0.502	H4	0.168	0.510	0.168
				O5	0.168	0.511	0.827	H5	0.167	0.513	0.500

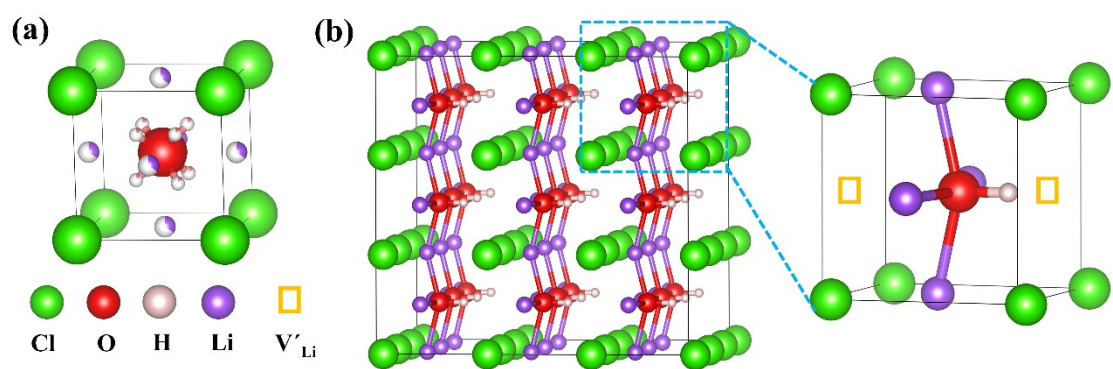


Figure S1. (a) The unrelaxed cubic phase of Li_2OHCl and (b) the relaxed ground-state structure of Li_2OHCl .

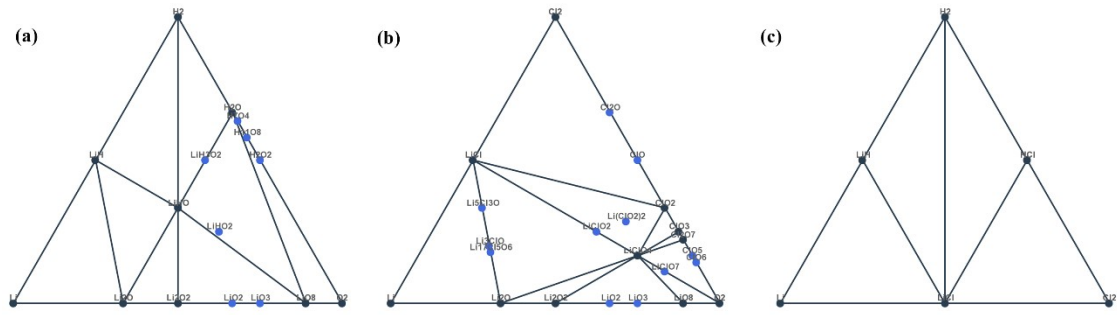


Figure S2. The phase diagram of the precursors adopted in the synthesis of protonated anti-perovskite (Li_2OHCl), the results are generated by Material Project[16].

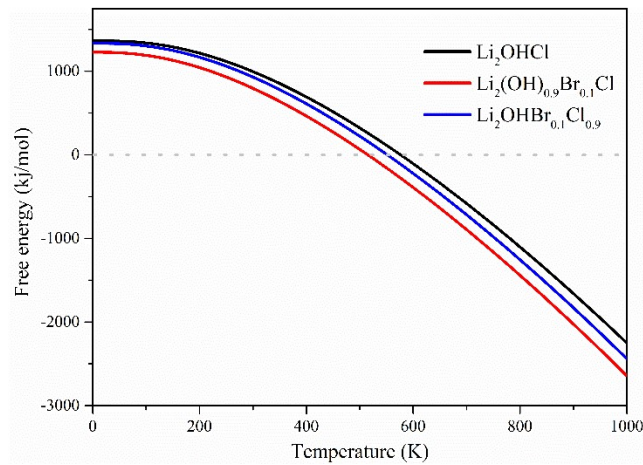


Figure S3. Helmholtz free energies by the vibrational entropy for Li_2OHCl , $\text{Li}_2(\text{OH})_{0.9}\text{Br}_{0.1}\text{Cl}$ and $\text{Li}_2\text{OHBr}_{0.1}\text{Cl}_{0.9}$.

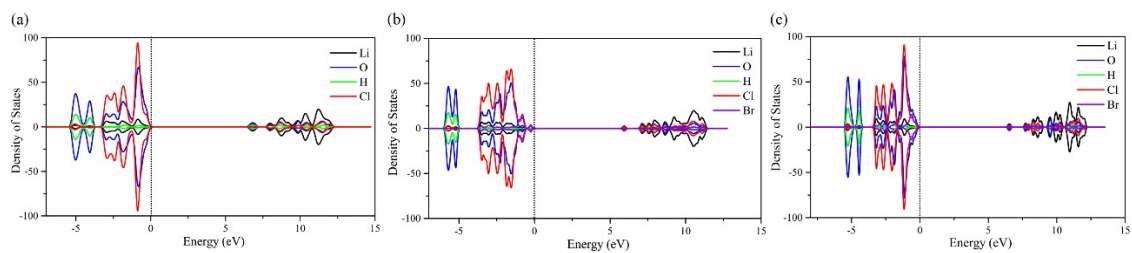


Figure S4. The partial density of states (pdos) for (a) Li_2OHCl , (b) $\text{Li}_2(\text{OH})_{0.9}\text{Br}_{0.1}\text{Cl}$ and (c) $\text{Li}_2\text{OHBr}_{0.1}\text{Cl}_{0.9}$, black, blue, green, red and purple lines represent the pdos of lithium, oxygen, hydrogen, chlorine elements, respectively.

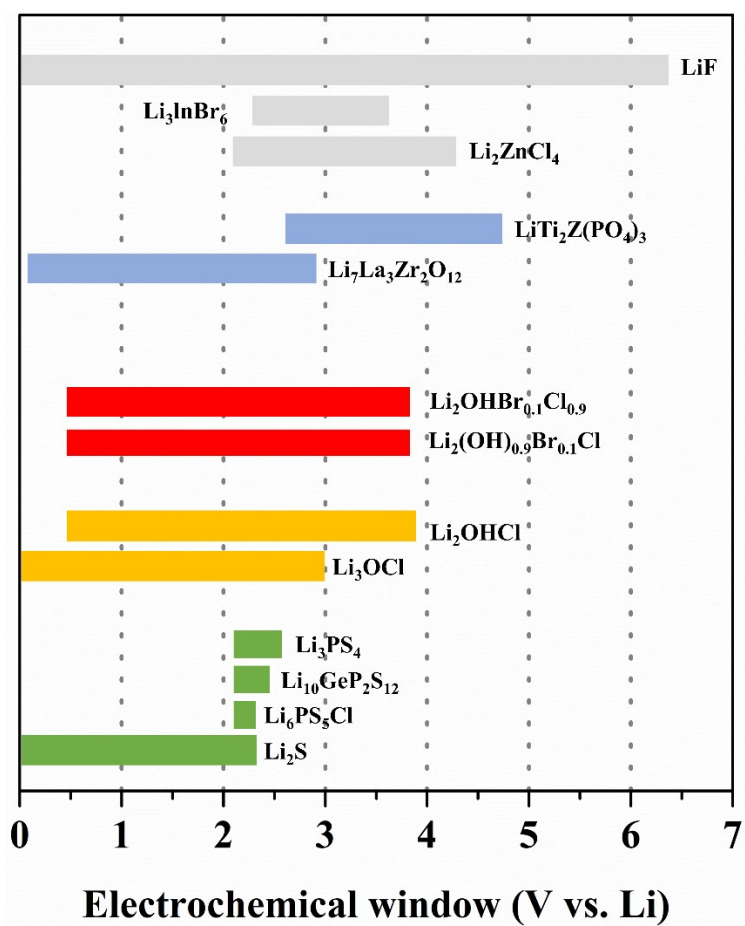


Figure S5. The electrochemical windows of normal solid state electrolytes.

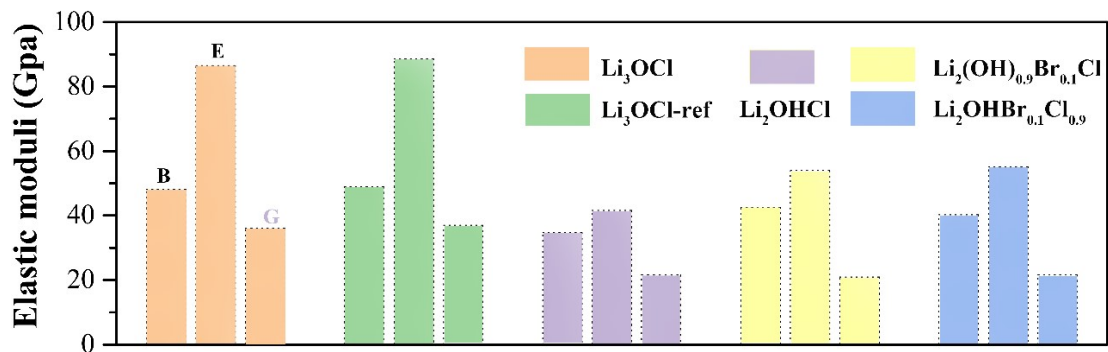


Figure S6. The calculated B, E and G for Li₃OCl, Li₂OHCl, Li₂(OH)_{0.9}Br_{0.1}Cl and Li₂OHBr_{0.1}Cl_{0.9}, respectively. The Li₃OCl-ref represents the values reported by reference of 36.

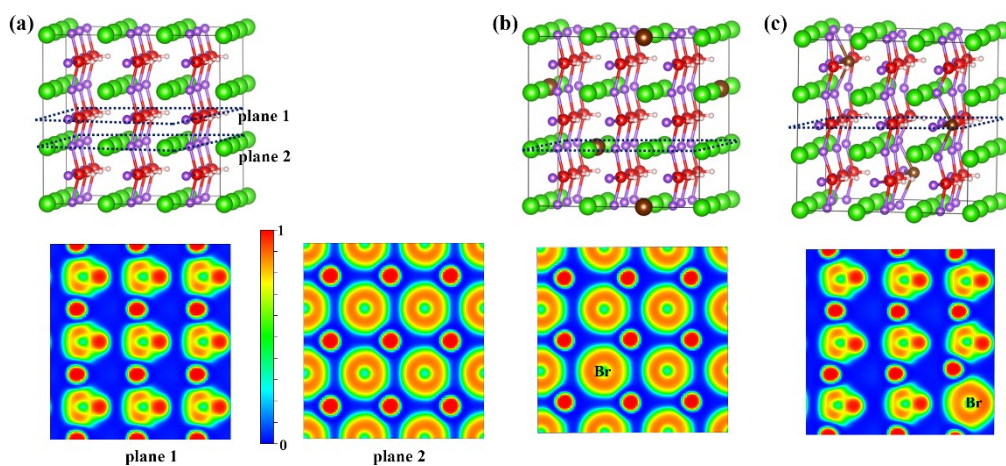


Figure S7. The electron localization function (ELF) of (a) Li_2OHCl , (b) $\text{Li}_2\text{OHBr}_{0.1}\text{Cl}_{0.9}$ and (c) $\text{Li}_2(\text{OH})_{0.9}\text{Br}_{0.1}\text{Cl}$, the black frame represents the corresponding plane for the ELF.

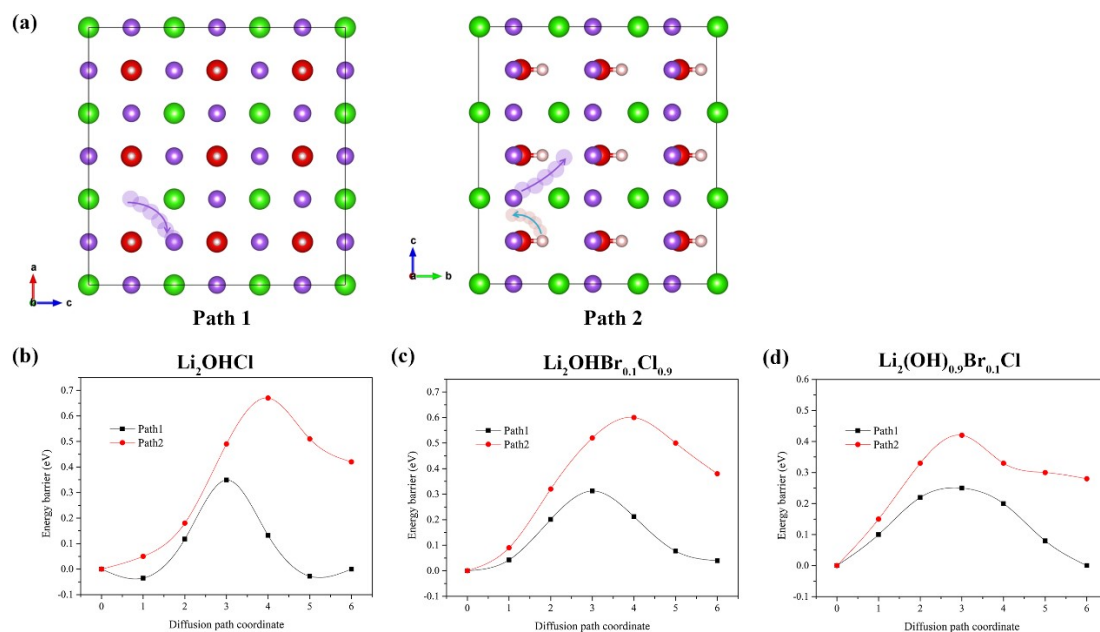


Figure S8. (a) The diffusion paths for neb calculations. (b-d) represents the corresponding diffusion barriers for Li_2OHCl , $\text{Li}_2\text{OHBr}_{0.1}\text{Cl}_{0.9}$ and $\text{Li}_2(\text{OH})_{0.9}\text{Br}_{0.1}\text{Cl}$ along path1 and path2, respectively.

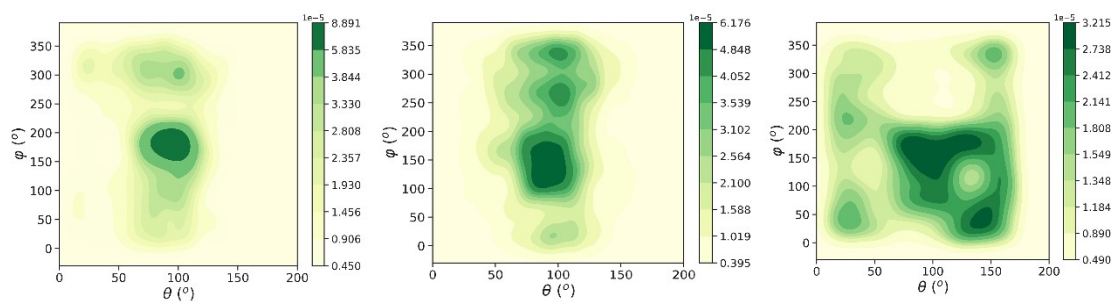


Figure S9. 2D projected probability distribution of H ligand bonded to O, representing the Li_2OHCl , $\text{Li}_2\text{OHBr}_{0.1}\text{Cl}_{0.9}$ and $\text{Li}_2(\text{OH})_{0.9}\text{Br}_{0.1}\text{Cl}$, respectively. Definition of the angles θ and Φ in the reference frame of the crystal lattice, with θ defined as the angle between the O–H bond and z axis and the angle Φ corresponding to the angle between the x axis and the projection of the O–H vector in the xy plane.

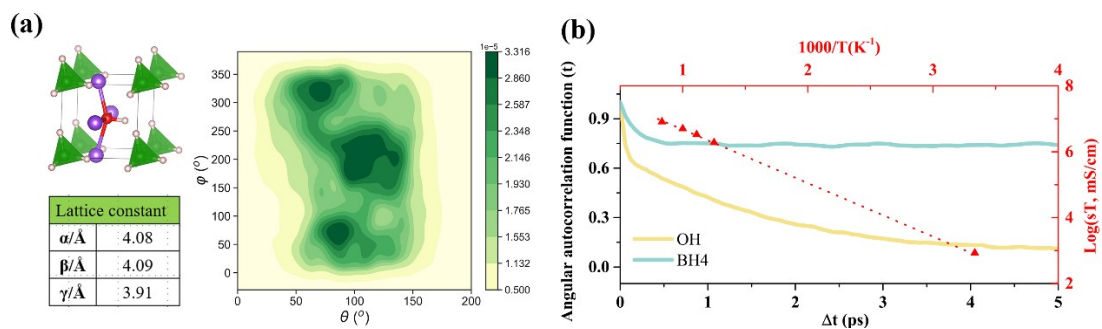


Figure S10. (a) The optimized structure and the corresponding lattice constant of the novel SSE. The right plane shows the 2D projected probability distribution of H ligand bonded to O. (b) displays the angular autocorrelation function for OH, BH₄ groups and the derived Arrhenius plot of the novel SSE. (red line).

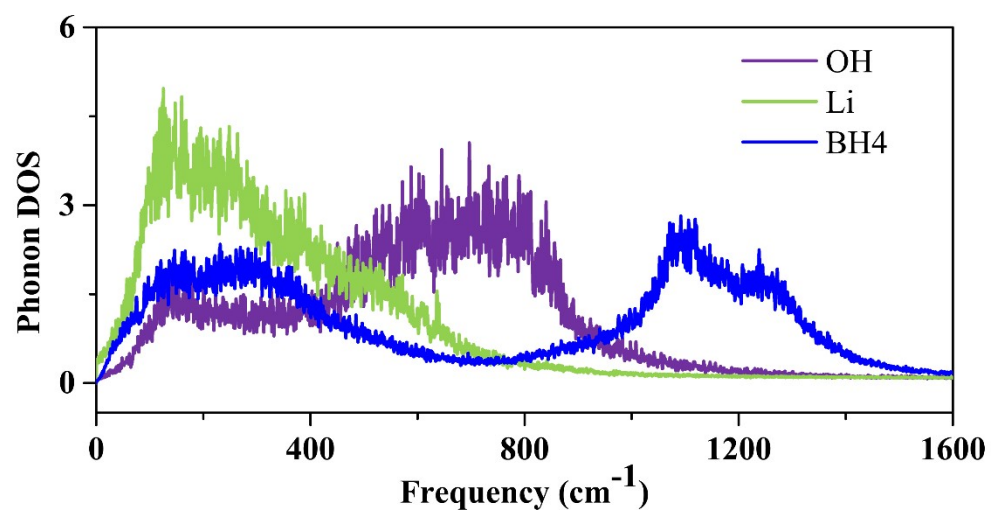


Figure S11. The vibrational spectrum (phonon DOS) of OH, Li and BH₄ in Li₂OHBH₄ during AIMD simulation.

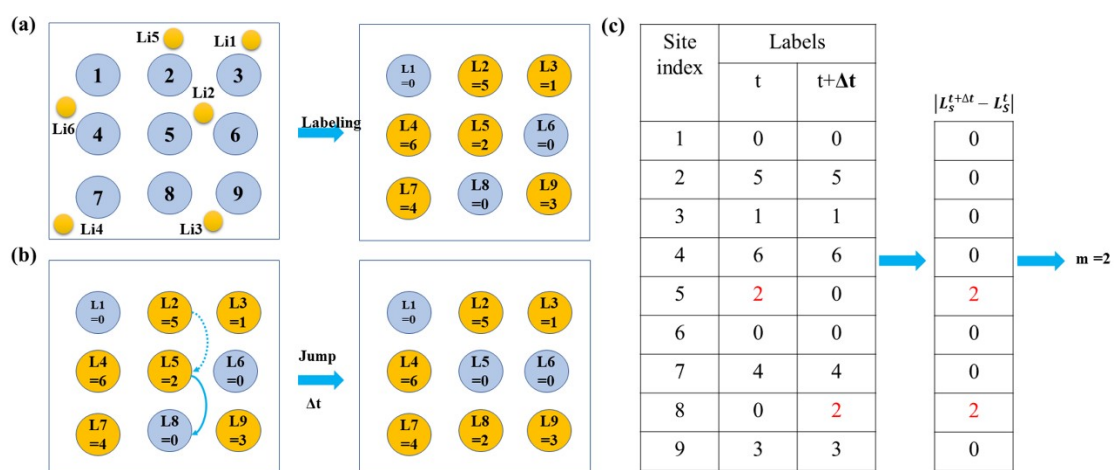


Figure S12 Analysis of the Li trajectories from AIMD simulations. (a) schematic illustrating the labeling process, (b) and (c) the determination jumps.

References

- [1] I. Hanghofer, G.J. Redhammer, S. Rohde, I. Hanzu, A. Senyshyn, H.M.R. Wilkening, D. Rettenwander, Untangling the Structure and Dynamics of Lithium-Rich Anti-Perovskites Envisaged as Solid Electrolytes for Batteries, *Chemistry of Materials*, 30 (2018) 8134-8144.
- [2] S.P. Ong, W.D. Richards, A. Jain, G. Hautier, M. Kocher, S. Cholia, D. Gunter, V.L. Chevrier, K.A. Persson, G. Ceder, Python Materials Genomics (pymatgen): A robust, open-source python library for materials analysis, *Computational Materials Science*, 68 (2013) 314-319.
- [3] J.A. Dawson, T.S. Attari, H. Chen, S.P. Emge, K.E. Johnston, M.S. Islam, Elucidating lithium-ion and proton dynamics in anti-perovskite solid electrolytes, *Energy & Environmental Science*, 11 (2018) 2993-3002.
- [4] C. Chen, W. Ye, Y. Zuo, C. Zheng, S.P. Ong, Graph Networks as a Universal Machine Learning Framework for Molecules and Crystals, *Chemistry of Materials*, 31 (2019) 3564-3572.
- [5] L.W. Shyue Ping Ong, Byoungwoo Kang, and Gerbrand Ceder, Li-Fe-P-O₂ Phase Diagram from First Principles Calculations, *Chem. Mater.*, 20 (2008) 1798-1807.
- [6] P. Deák, B. Aradi, T. Frauenheim, Polaronic effects in TiO₂ calculated by the HSE06 hybrid functional: Dopant passivation by carrier self-trapping, *Physical Review B*, 83 (2011).
- [7] A. Urban, D.-H. Seo, G. Ceder, Computational understanding of Li-ion batteries, *npj Computational Materials*, 2 (2016).
- [8] P. Peljo, H.H. Girault, Electrochemical potential window of battery electrolytes: the HOMO-LUMO misconception, *Energy & Environmental Science*, 11 (2018) 2306-2309.
- [9] H. Tang, Z. Deng, Z. Lin, Z. Wang, I.-H. Chu, C. Chen, Z. Zhu, C. Zheng, S.P. Ong, Probing Solid-Solid Interfacial Reactions in All-Solid-State Sodium-Ion Batteries with First-Principles Calculations, *Chemistry of Materials*, 30 (2017) 163-173.
- [10] Z. Deng, Z. Wang, I.-H. Chu, J. Luo, S.P. Ong, Elastic Properties of Alkali Superionic Conductor Electrolytes from First Principles Calculations, *Journal of The Electrochemical Society*, 163 (2015) A67-A74.
- [11] B. Ouyang, Y. Wang, Y. Sun, G. Ceder, Computational Investigation of Halogen-Substituted Na Argyrodites as Solid-State Superionic Conductors, *Chemistry of Materials*, 32 (2020) 1896-1903.
- [12] N.J.J. de Klerk, E. van der Maas, M. Wagemaker, Analysis of Diffusion in Solid-State Electrolytes through MD Simulations, Improvement of the Li-Ion Conductivity in beta-Li₃PS₄ as an Example, *ACS Appl Energy Mater*, 1 (2018) 3230-3242.
- [13] N.J.J. de Klerk, I. Rosłoń, M. Wagemaker, Diffusion Mechanism of Li Argyrodite Solid Electrolytes for Li-Ion Batteries and Prediction of Optimized Halogen Doping: The Effect of Li Vacancies, Halogens, and Halogen Disorder, *Chemistry of Materials*, 28 (2016) 7955-7963.
- [14] <aesr.202000101.pdf>.
- [15] Z. Zhang, P.N. Roy, H. Li, M. Avdeev, L.F. Nazar, Coupled Cation-Anion Dynamics Enhances Cation Mobility in Room-Temperature Superionic Solid-State Electrolytes, *Journal of the American Chemical Society*, 141 (2019) 19360-19372.
- [16] M. de Jong, W. Chen, T. Angsten, A. Jain, R. Notestine, A. Gamst, M. Sluiter, C. Krishna Ande, S. van der Zwaag, J.J. Plata, C. Toher, S. Curtarolo, G. Ceder, K.A. Persson, M. Asta, Charting the complete elastic properties of inorganic crystalline compounds, *Sci Data*, 2 (2015) 150009.